

Article

Can We Detect the Brownness or Greenness of the Congo Rainforest Using Satellite-Derived Surface Albedo? A Study on the Role of Aerosol Uncertainties

Suman Moparthy, Dominique Carrer * and Xavier Ceamanos

CNRM, Université de Toulouse, Météo-France, CNRS. 42 Avenue Gaspard Coriolis, 31057 Toulouse, France; suman.moparthy@meteo.fr (S.M.); xavier.ceamanos@meteo.fr (X.C.)

* Correspondence: dominique.carrer@meteo.fr

Received: 31 January 2019; Accepted: 1 March 2019; Published: 6 March 2019



Abstract: The ability of spatial remote sensing in the visible domain to properly detect the slow transitions in the Earth's vegetation is often a subject of debate. The reason behind this is that the satellite products often used to calculate vegetation indices such as surface albedo or reflectance, are not always correctly decontaminated from atmospheric effects. In view of the observed decline in vegetation over the Congo during the last decade, this study investigates how effectively satellite-derived variables can contribute to the answering of this question. In this study, we use two satellite-derived surface albedo products, three satellite-derived aerosol optical depth (AOD) products, two model-derived AOD products, and synthetic observations from radiative transfer simulations. The study discusses the important discrepancies (of up to 70%) found between these satellite surface albedo products in the visible domain over this region. We conclude therefore that the analysis of trends in vegetation properties based on satellite observations in the visible domain such as NDVI (normalized difference vegetation index), calculated from reflectance or albedo variables, is still quite questionable over tropical forest regions such as the Congo. Moreover, this study demonstrates that there is a significant increase (of up to 14%) in total aerosols within the last decade over the Congo. We note that if these changes in aerosol loads are not correctly taken into account in the retrieval of surface albedo, a greenness change of the surface properties (decrease of visible albedo) of around 8% could be artificially detected. Finally, the study also shows that neglecting strong aerosol emissions due to volcano eruptions could lead to an artificial increase of greenness over the Congo of more than 25% in the year of the eruptions and up to 16% during the 2–3 years that follow.

Keywords: vegetation; surface albedo; aerosol optical depth; greenness; brownness; Congo; MODIS; MISR; SEVIRI; MERRA; CAMS

1. Introduction

Tropical rainforests play a crucial role in the regulation of regional climate and weather worldwide owing to their close interaction with the hydrological cycle [1,2]. They assist in the upward transport of moisture through the process of evapotranspiration that increases the chance of precipitation [1] and thus favoring the vegetation growth. A reduced forest cover mitigates this process and results in perturbed rainfall patterns [3]. Furthermore, the indirect effects of atmospheric aerosols adversely impact clouds and in turn precipitation, which is pivotal for vegetation growth. Anthropogenic activities like forest-clearing fires and the burning of the savanna for colonization and agriculture creates air pollution which releases biomass aerosol particles into the atmosphere, that later directly interact with solar radiation by the process of scattering and absorption [4]. Biomass-burning aerosols contribute to increasing cloud formation but somewhat paradoxically also to decreasing rainfall [5,6].

The smaller cloud size droplets created by smoke particles cannot grow to sizes sufficiently large enough for precipitation [7]. This reduction in rainfall leaves the burnt forest areas more susceptible to further dryness and fires [8] and hence result in a less vegetation growth. The greenness reflects the increase of vegetation over the rainforest and it is therefore indirectly a measure of the health of the rainforest. The increase or decrease of forest canopy can result in greenness (decrease in surface reflectance and albedo) or brownness (an increase in surface reflectance and albedo), respectively [9]. Surface albedo values are usually low over thick rainforests as and when compared to non-vegetated surfaces [1].

Satellite observations used to derive vegetation indices help to characterize and monitor the forest vegetation on Earth [3], which is crucial for achieving sustainable forest management [10]. The surface information in the spectral channels in the visible (VIS; 0.4–0.7 μm) and near-infrared (NIR; 0.8–2.5 μm) spectral domains that are used to derive these indices is often contaminated by the extinction effects of aerosols and clouds due to limited atmospheric correction [11]. In this manuscript, the emphasis is put on the residual contamination due to aerosols and their impact on the surface reflectance or albedo satellite products. Studies conducted by Franch et al. [12] showed that the presence of high aerosol loads may introduce large errors in the computation of surface reflectivity properties. Their study showed that the presence of scattering aerosols can induce positive changes in derived albedo compared to absorbing aerosols, which may induce negative changes. This link between surface and aerosol properties drives the scientific community to perform an exact estimation of aerosol load and type for a proper atmospheric correction [11].

In spite of the best efforts made by the scientific community, however, there still remain inconsistencies in the satellite retrievals. This adversely impacts the quality of the estimated aerosol load [13,14] which is otherwise important in atmospheric correction. In line with this, some studies discuss the inaccuracies in surface observations due to the limitations in the retrieval of the proper aerosol load [15–19]. For example, Kim et al. [15] showed that a 1% error in surface reflectance could result in a 10% error for the aerosol optical depth (AOD). Another study by Seidel and Popp [17] showed similar results in the presence of dust particles in the atmosphere. Hence, the determination of the realistic aerosol load and type is crucial for an accurate atmospheric correction of surface reflectance. This is in turn used in the estimation of essential climate variables such as surface albedo and vegetation indices [20]. However, studies admit that complete atmospheric correction of aerosols on an operational basis is difficult and there always remains some aerosol contamination in the observed satellite reflectance [11]. It is worth discussing here that temporal averaging can help to reduce the residual errors. For example, the satellite albedo products have different characteristic time scales comprised between 1 day and 30 days. The longer the composite period, the lower the atmospheric residual contamination should be in the satellite albedo products. However, the impact is more visible in terms of standard deviation of the statistical scores (but may be less in the case of bias statistics). In any case, several communities working in climate groups and Numerical Weather Prediction (NWP) express the need for daily estimates.

Many studies show a decline in the greenness of vegetation over Amazonian and African rainforests based on satellite observations [20–24]. These studies draw important conclusions on the health of forest vegetation in terms of the increasing brownness of the forest cover. The tropical forest in the democratic republic of Congo was found to be more tolerant of the short-term deficit in rainfall as compared to the Amazonian forest [3]. Longer droughts have however transformed the canopy architecture from much denser to sparse [3] which has a profound impact on the surface albedo of the canopy [25]. It is important to note that the saturation of the surface signal in the band ratio of VIS to NIR is a known problem [26,27]. This is due to the fact that the vegetation indices are based on the absorption properties in VIS and NIR domains and sometimes over the thick forests, the red channel in VIS band sense very low values leading to saturation. In this context, it is important for the scientific community to better characterize the decline of vegetation from the observed changes in the surface albedo. Usually, the vegetation indices are considered as a good proxy for monitoring

the growth of vegetation and for the detection of surface changes [23]. Nevertheless, the studies which highlight the possible modifications of the vegetation of forests from vegetation indices could be jeopardized by several factors such as viewing geometry, residual clouds and more significantly aerosol contamination [12,15,21,28]. Research conducted by Anderson et al. [22] reports that there were several limitations associated with the usage of NDVI (normalized difference vegetation index) as a proxy for identifying the health of green vegetation due to its sensitivity to atmospheric aerosols and soil background. Furthermore, they suggest the use of EVI (enhanced vegetation index) and NDWI (normalized difference water index) as an alternative to NDVI for a better understanding of vegetation characteristics [22]. In any case, all these indices are calculated based on the surface parameters that may still be contaminated by aerosols.

As mentioned previously, accurate knowledge of aerosol conditions is important considering their role in atmospheric correction. The greenness of vegetation is associated with a decrease in albedo in the visible domain, where vegetation absorbs the light mainly in the blue and red wavelengths to trigger photosynthesis. The healthier the vegetation, the larger the quantities of absorbed photons in the VIS domain on the solar spectrum, thereby leading to a decrease in the associated albedo. Conversely, brownness of vegetation leads to an increase in the VIS surface albedo. The NIR domain is not affected by the photosynthesis process and hence the impact of greenness or brownness on surface albedo is lower. It is worth discussing again that greenness or brownness affect the calculation of NDVI as they are based on the normalized difference between visible and near-infrared signals [29]. In this study, we conduct an analysis in order to answer the following question: What could we expect nowadays to detect from satellite-derived surface albedo for the analysis of temporal shifts in vegetation? This is done by paying particular attention to the uncertainty due to the misunderstanding of aerosol load, especially in the visible domain. In other words, it is important to ascertain whether or not the detected changes of brownness or greenness are not simply the result of a false atmospheric correction due to an incorrect knowledge of the aerosol load.

The region of interest for this study is the Congo rainforest in Africa [3], where earlier studies showed a decline in vegetation leading to a browning phase [3]. We focus our analysis on the surface albedo observed in the VIS and NIR domains. The first objective of the study is to analyze whether or not an agreement between the different high-quality satellite-based albedo products over Congo exists. The second objective is to discuss if the potential disagreement is due to the differences in the aerosol optical depth products that are used for atmospheric correction. Reanalysis aerosol optical depth data from two atmospheric models, as well as AOD records from various space-borne sensors aboard polar and geostationary platforms are considered for the purpose of this study.

The present article is organized as follows. Section 2 presents the data and methodology. The results are discussed in Section 3. Section 4 summarizes and Section 5 concludes the study while putting emphasis on future perspectives.

2. Materials and Methods

2.1. Surface Albedo

In this study we consider two satellite-derived bi-hemispherical surface albedo products in the VIS and NIR domains for the year 2014. Surface albedo is estimated from (i) observations based on the camera moderate resolution imaging spectroradiometer (MODIS) aboard the polar orbiting satellites Terra and Aqua, and (ii) observations from the camera Spinning Enhanced Visible and Infrared Imager (SEVIRI) aboard the geostationary satellite Meteosat Second Generation. Hereafter unless specified otherwise, we refer to MODIS and SEVIRI surface albedo products in their appropriate contexts.

For MODIS, the surface albedo data from Terra and Aqua satellites are merged to produce a 16-day composite of albedo at a 1 km resolution. This product (MCD43B3) is interpolated and distributed on an 8-day basis. The method for its retrieval and the full technical specifications are found in [30–34].

MODIS satellite reflectances are corrected for aerosol effects using a continental aerosol model and MODIS aerosol optical depth product before deriving the surface albedo product [35,36].

For SEVIRI, the chosen product is the land surface albedo product [30,31] provided by the LSA-SAF project (<http://lsa-saf.eumetsat.int/>). The spatial resolution of this product is around 3 km for the Congo region and a map of surface albedo is retrieved on a daily basis. The atmospheric correction uses the AOD climatology which was basically derived from the value of latitude [30]. The type of aerosol is also assumed to be continental (as is that of MODIS) [30].

In the past, Carrer et al. [31] exposed a reasonably good agreement between MODIS and SEVIRI for both visible (with 20% uncertainty) and NIR albedo (with 5% uncertainty). The higher uncertainty observed in the visible band may occur due to the sensitivity of atmospheric aerosols in this band.

2.2. Aerosol Optical Depth

2.2.1. Satellite-Based Products

Three satellite AOD products are used in our study. These products are based on observations from three satellite sensors namely: SEVIRI, MODIS and MISR. MISR is also aboard the Terra polar-orbiting satellite. The AOD retrieval method for MODIS uses a bi-modal aerosol distribution with three models for fine mode aerosol and a dust model for the coarse mode aerosol [37]. The MODIS AOD used in the study is at wavelength 0.55 μm from the latest collection-6 product [37] and collection-5.1 product [38]. The MODIS collection-6.0 product employs both the deep blue algorithm and dark target algorithms for the expansion of aerosol retrievals across all surfaces [37]. Unless specified otherwise, we represent the collection-6 MODIS products with 'C-6' and collection-5.1 MODIS AOD product with 'C-5.1'. The Dark Target method is employed for MODIS AOD retrievals over vegetated and dark soil regions such as the Congo [37]. The error in AOD for MODIS as reported by Levy et al. [37] is $\pm 0.05 + 0.15$.

AOD retrieved from Multi-angle Imaging Spectroradiometer (MISR) uses the directional information of aerosol and surface reflectance from nine cameras arranged within 0 to 70° on either side of the nadir view. The aerosol properties are measured by comparing the measured radiance at the top of the atmosphere (TOA) with the radiances that are pre-computed using several aerosol models [39]. We used AOD at 0.558 μm from MISR for the current study. The overall accuracy of MISR AOD is about 0.05 according to Reference [40].

The method to derive AOD from SEVIRI observations is called AERUS-GEO (aerosol and surface albedo retrieval using a directional splitting method-application to GEOstationary data) and is detailed in [41,42]. Aerosol properties are derived by examining the temporal evolution of the directionality of the satellite observations [41]. SEVIRI AOD is derived at the wavelength of 0.63 μm . The aerosol type is estimated thanks to an iterative procedure described in Reference [42]. Xu et al. [43] and Nabat et al. [44] show the accuracy of SEVIRI AOD to be comparable to MODIS and MISR products. In the current study, unless and otherwise specified we refer to the AOD product from MSG SEVIRI as SEVIRI AERUS GEO.

2.2.2. Aerosol Products from Atmospheric Modeling

In this study, we have also considered the AOD from the Copernicus Atmospheric Monitoring Service (CAMS) near real-time products and from modern era retrospective-analysis for research and applications (MERRA) reanalysis products. The validation of CAMS aerosol products and others are reported in [45,46] where the AOD at 550 nm is evaluated in conjunction with AERONET (aerosol robotic network) ground measurements. The overall bias on average was found to be 20%, which decreased to 5% in winter, by Eskes et al. [45]. In another study [47], the bias on average was found to vary by up to 30% during the summer of 2016 from a comparison observed between CAMS AOD at 550 nm and AERONET observations. The MERRA reanalysis model aerosol data is taken from the GIOVANNI online data system (as observed from the web source; <https://giovanni.gsfc.nasa.gov/giovanni>) [48]. MERRA reanalysis model AOD data consider the aerosol components such as dust, sea

salt, black carbon, organic carbon and sulfate. All aerosol components are considered to be externally mixed [49]. The sulfate and carbon components of aerosols are assumed to be fine mode whereas the sea salt (with five size bins between 0.03 and 10 μm) and dust (with five size bins between 0.1 and 10 μm) are assumed to both fine mode and coarse mode [49]. The sources of aerosols in the model are based on wind-speed emissions of dust and sea salt, fossil fuel, biomass burning, biofuel consumption, biogenic particulate matter, oxidation of dimethyl sulfide and SO_2 . The model sources also include volcanic sources [49]. More information on the model and aerosol sinks are found in Reference [49] (and references therein).

In addition, the MERRA aerosol products have been extensively validated and employed among the scientific community [50–52]. MERRA AOD at 440 nm yields a correlation coefficient of 0.69 along with a positive bias of 0.20 when compared in conjunction with the AERONET observations over the Sahara and the North Atlantic Ocean [52].

2.3. Spectral, Spatial and Temporal Reprojection

The AOD product from SEVIRI AERUS GEO has a finer spatial resolution (3 km from the equator) compared to MODIS and MISR AOD products. MODIS aerosol data have a grid resolution of nearly 11 km, whereas a MISR level 3 daily product has a resolution of nearly 55 km. Hence, it was necessary to re-grid SEVIRI AERUS GEO AOD data to the corresponding grid resolution of MODIS and MISR for the purpose of comparison. Concerning the differences of spectral characteristics of the different satellite products (AOD at 0.63, 0.55, and 0.58 μm) for MSG SEVIRI, MODIS and MISR respectively, we arbitrarily decide to keep these products as they are, since spectral conversions would have required a proper knowledge of the aerosol type.

Regarding surface albedo, SEVIRI albedo was also averaged across the same MODIS 8-day periods.

2.4. Experimental Setup

The first step of this study is to verify whether or not there is a good spatial agreement between SEVIRI and MODIS albedo products over the tropical rain forest region of Congo. Spatial maps of AOD bias observed from several satellite products are then examined over the same region. The goal here is to observe and understand whether or not differences in the AOD products could explain those observed differences in the albedo maps. At a later stage, we use a radiative transfer model to estimate and discuss the uncertainty on albedo retrieval with respect to the differences in AOD. Model-based AOD data from MERRA and CAMS corroborate our findings. We also assess the long term analysis of MERRA AOD between 1980 and 2016 for various aerosol types and try to explain if any trend in the AOD observed could explain the uncertainties of albedo.

3. Results and Discussion

3.1. AOD and Surface Albedo Observations over the Study Area

Study Area. The study is conducted over the region of Congo, Africa (14° E to 30° E; −7° S to 5° N). Shown in Figure 1 is the ESA-CCI land cover product derived land cover map (<http://maps.elie.ucl.ac.be/CCI/viewer/index.php>) zoomed over the region of Congo.

From Figure 1 it can be observed that vegetation is dominated by broadleaved evergreen forest in the north of the Congo whereas crops dominate the southern part.

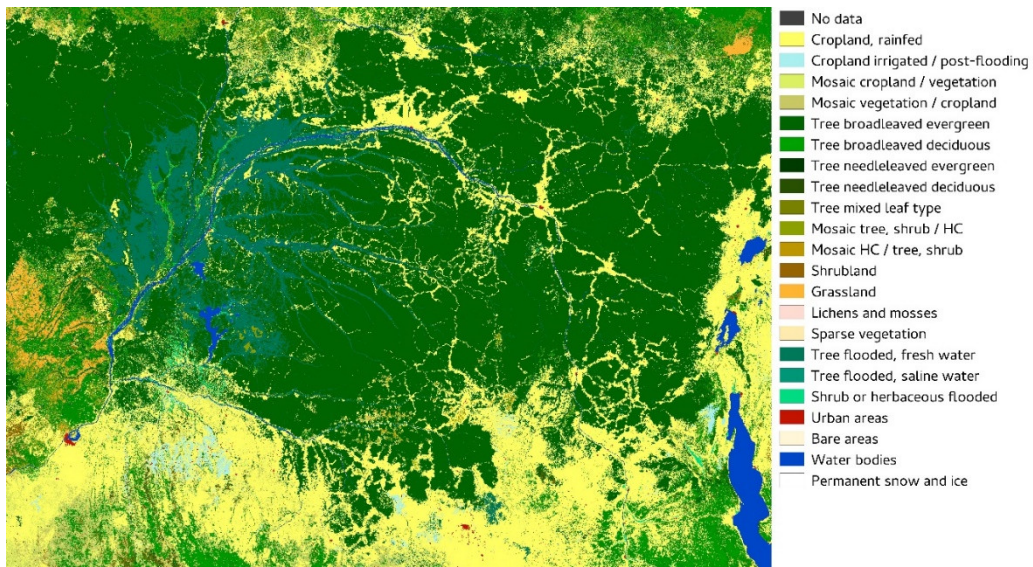


Figure 1. Land cover as observed from European Space Agency (ESA) Climate Change Initiative (CCI), ESA-CCI for 2010 zoomed over the region of Congo, Africa. The legend of the various land cover types is shown in the figure.

Mean surface albedo observations for 2014. The mean surface albedo values as observed from MODIS and SEVIRI during the year 2014 over the region of Congo are shown in Figure 2. Albedo values are shown for both the VIS and NIR domains.

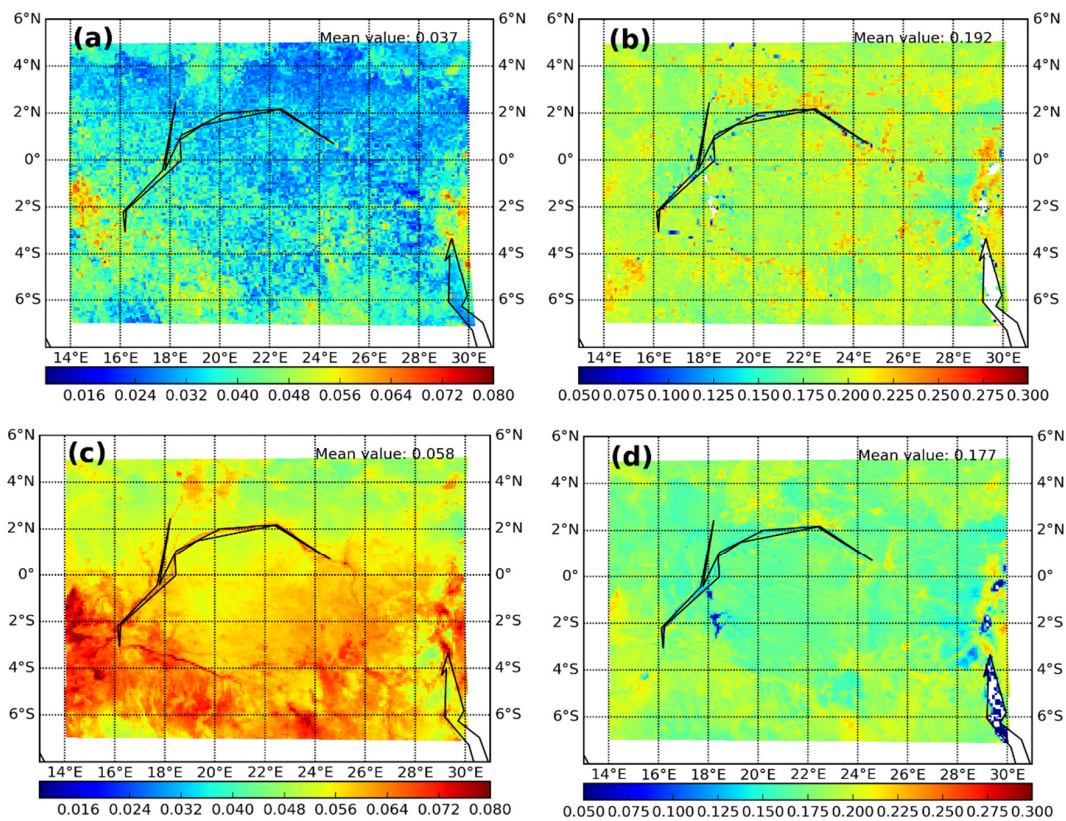


Figure 2. Spatial distribution of the mean surface albedo values in (a) VIS and (b) NIR as observed from MODIS combined data and in (c) VIS and (d) NIR as observed from SEVIRI during the period 2014 over the region of Congo, Africa. The black lines delineate the water bodies, the Congo river in the middle and the lakes Kivu, Edward and Tanganyika on the extreme bottom right.

From the figure above, we observe that the mean VIS albedo in 2014 is lower in the northern Congo over forest cover type and higher in the south over crop cover type. Such contrast from northern to southern regions is not as obvious in the NIR domain. The mean VIS albedo values as observed from SEVIRI (mean value of 0.06) are higher compared to MODIS (mean value of 0.04). The differences in NIR surface albedo as observed from SEVIRI (mean value of 0.18) compared to MODIS (mean value of 0.19) are not as significant. Compared to the NIR domain, the visible domain is more sensitive to atmospheric contamination due especially to the presence of aerosols.

Variation of aerosol optical depth and its associated trends for the last three decades. In this section, the temporal and spatial variations of AOD over the region of the Congo are shown and are discussed. Later, we show the time series of MERRA AOD for the last 3 decades and discuss any observed potential trends. Figure 3 shows the daily temporal variation of MERRA model AOD with respect to other satellite and CAMS model AOD products over the region of the Congo during the year 2014. The time series is constructed by considering the average spatial value of AOD over the study region. We observe a good temporal correlation between MERRA and other AOD products. It is also observed from the figure that all satellite and model AOD products record high AOD values over the study region suggesting that the study region is prone to high aerosol episodes, especially during the period of June to September.

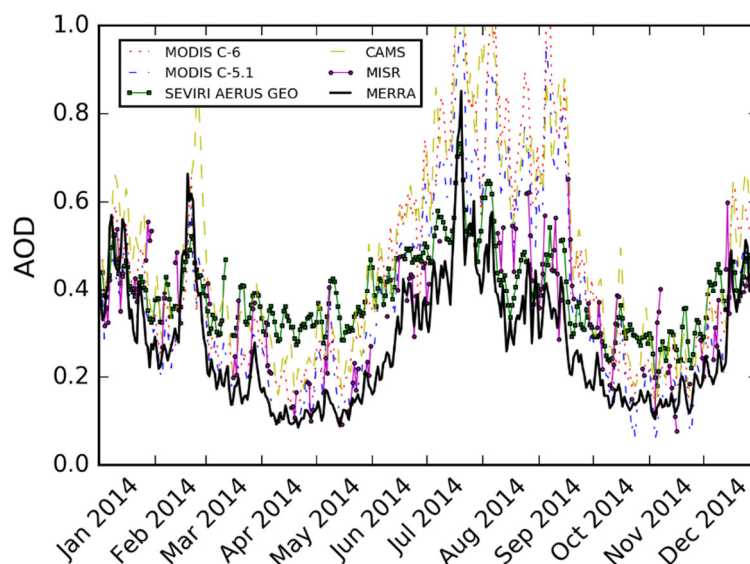


Figure 3. Temporal Variations of the aerosol optical depth (AOD 550 nm) over the region of Congo, during the year 2014 between MERRA model AOD and various satellite AOD products (MODIS collection 6 and 5.1, SEVIRI AERUS GEO and MISR) and model AOD from CAMS.

The statistics of comparison between the satellite-derived AOD and MERRA model AOD are shown in Table 1.

Table 1. Statistics of comparison between satellite-derived AOD products (MODIS collection 5.1 and 6, SEVIRI AERUS GEO, MISR) and CAMS model AOD with respect to MERRA model AOD. The statistics are prepared considering data points of MERRA over a daily basis.

Serial No	AOD Product Satellite/Model	Statistics of Comparison				
		RMSE	MBE	No of Points	R-Value	MEAN AOD
1	MODIS-6	0.23	−0.16	362	0.78	0.44
2	MODIS-5.1	0.14	−0.01	357	0.80	0.37
3	SEVIRI AERUS GEO	0.08	−0.11	362	0.77	0.39
4	MISR	0.08	−0.08	268	0.60	0.34
5	CAMS	0.28	−0.19	365	0.84	0.47

It is observed from Table 1 that the MERRA model AOD values are mostly negatively biased. The observed statistical scores (RMSE and MBE) from the table reveal that MERRA AOD is comparable in performance to satellite products MODIS collection 5.1, SEVIRI AERUS GEO and MISR, more so than AOD products observed from MODIS collection 6.0 and CAMS.

Figure 4 shows the mean AOD from the MERRA and CAMS data sets for the year 2014. It is observed from the figure that both CAMS and MERRA show similar spatial patterns for mean AOD observed at 550 nm, although mean AOD from CAMS (a value of 0.5) is higher than MERRA (a value of 0.3). The AOD values are observed to be higher in the southern and central part of the Congo region whereas the mean AOD values are relatively low in the northern region of the Congo. We note that the high AOD values in the south correspond to the urban and crop cover types and the low AOD values in the north correspond to the evergreen broadleaved trees and other dense vegetation cover types (see Figure 1). This dichotomy in AOD may be linked to the influence of the land cover type on the overlying AOD.

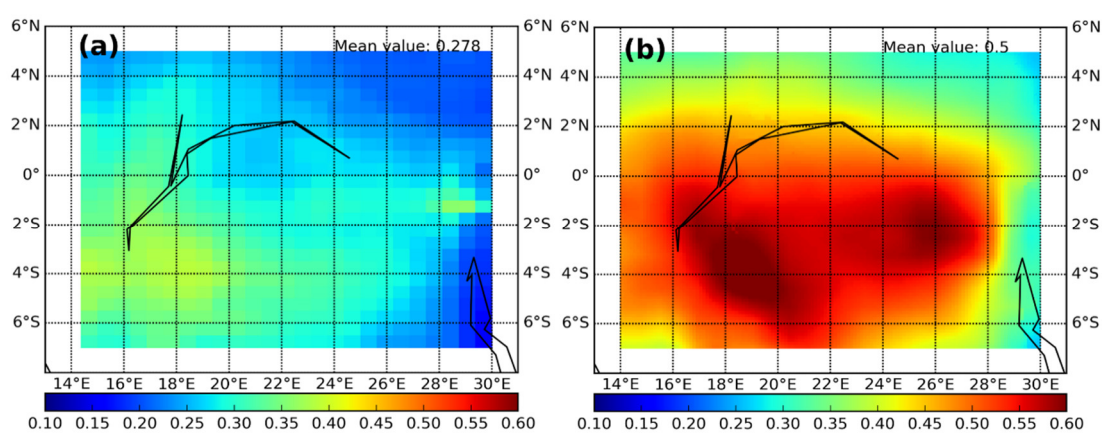


Figure 4. Spatial map of the aerosol optical depth (AOD 550 nm) over the region of the Congo, during the year 2014 for (a) MERRA and (b) CAMS. The black lines delineate the water bodies.

Shown in Figure 5a is the long term time series of aerosol load observed from MERRA for various particle types (namely, black carbon, dust, sea salt and sulfate) over the region of the Congo during the period 1980–2016. The black arrows in Figure 5 label the important volcanic eruption episodes observed during the study period. It is observed from Figure 5a that there is an increasing trend in the dust AOD. The Mann-Kendall test applied to the data set confirms this increasing trend. The dust AOD value in 2015 (0.06) is double the value observed in 1980 (0.03).

This increase in aerosol load over Africa due to dust was observed in earlier studies [53,54]. A modeling and observational study by Lee et al. Shows a high aerosol load over the democratic region of Congo (see Figure 6C in Reference [55]). In addition, in a modeling study conducted by Tummon et al. [56], it is hypothesized that low-level winds are significant for aerosol transport. This explains the high aerosol load observed in this study over the region [5° N to 15° S and 15° E to 30° E]. Furthermore, in the past decade (2005 to 2016), there was also an increase of total AOD by 14% (see Figure 5b regression line). The mean aerosol departure in the total AOD for the year 2014 with respect to the mean total AOD value for the entire period (0.32, shown by dotted black line Figure 5b) is around 14%. The increase in the total AOD during the last decade is partially attributed to the increasing contribution of black and organic carbon to the total AOD. It is to be underlined that the decline in vegetation over the Congo was indeed observed during the last decade (2000 to 2012) [3]. The lack of trend in the total AOD over the last three decades is due to the decreasing trend in the sulfate AOD, something compensated partially by an increasing trend in dust AOD. The decreasing trend in total aerosol load was indeed observed to be valid from the studies on multi-period decades as observed in most parts of the globe [53,54,57]. Finally, it can be reported that the impact of volcanic eruptions around the world on the mean AOD over the Congo is significant (Figure 5a, sulfate AOD

contribution in total AOD). Values can increase by up to 0.2 in the first year after the event and remain significant in the following 2 to 3 years with an increase in its value of 0.1.

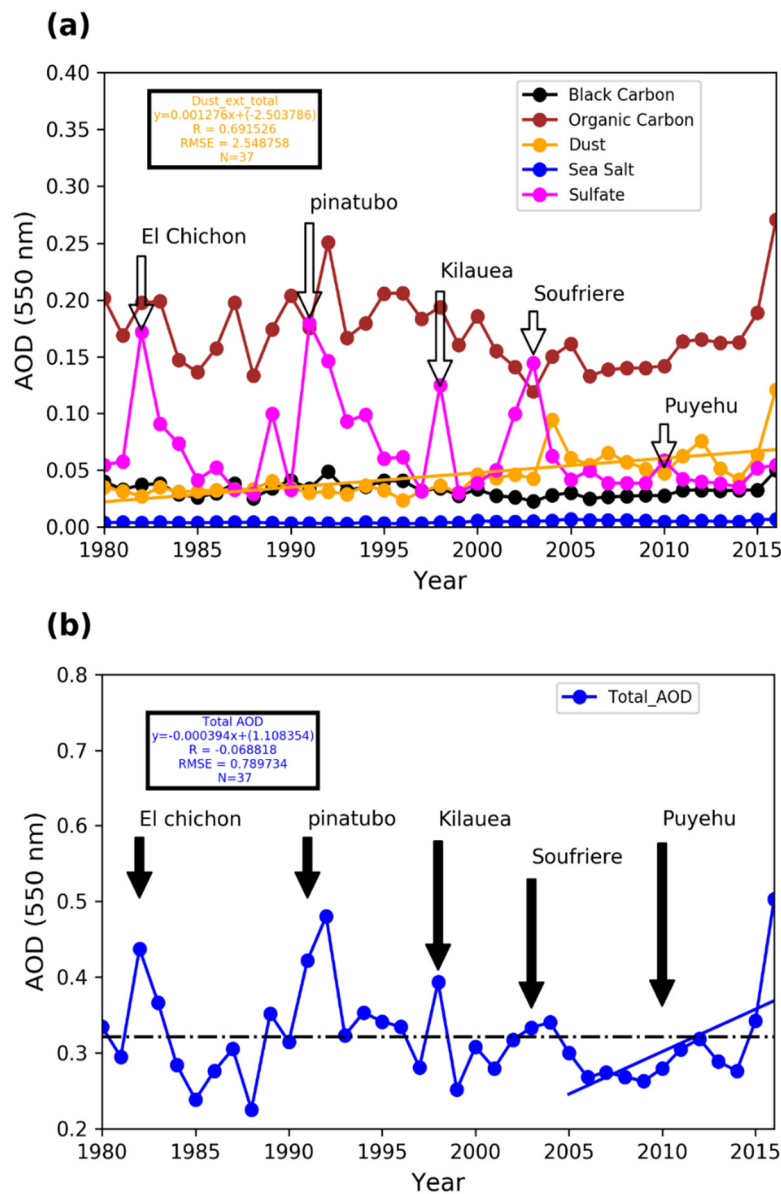


Figure 5. (a) Time series of AOD derived for different aerosol types namely Black Carbon, Dust, Sea Salt and Sulfate from MERRA reanalysis and (b) time series of total AOD over the region of Congo from MERRA reanalysis, for the period 1980–2016 over the region, Africa. The volcanic eruption episodes observed during the study period are indicated by downward arrows. The blue line (Figure 5b) shows the regression line for total AOD during the last decade. The dotted line in black (Figure 5b) shows the mean total AOD value computed for the entire period. The orange line (Figure 5a) shows the regression line for dust during the last 3 decades.

3.2. Differences between Satellite-Based Products

Satellite surface albedo products. In order to study the possible influence of wrong aerosol information on the satellite-derived surface albedo, a comparison is performed between the VIS and NIR surface albedo values of MODIS and SEVIRI as shown in Figure 6.

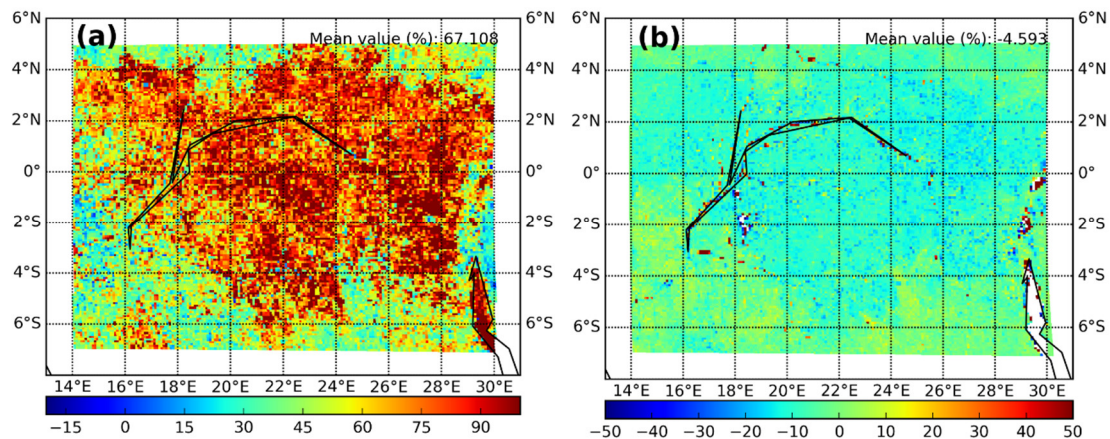


Figure 6. Spatial map of the mean relative differences (in %) between SEVIRI and MODIS albedos (SEVIRI-MODIS)/SEVIRI: (a) VIS domain and (b) NIR domain.

As can be observed from the figure, a north-south gradient is observed both in the VIS and NIR surface albedo. Differences between the two albedo products are much higher in the VIS domain, reaching a relative bias value of up to 70% over the major part of the region (Figure 6a). The observed maximum differences in the VIS domain suggest that the observed changes are sensitive to alterations in the atmospheric aerosols. The bias in the NIR domain is significantly lower, in spite of the likely presence of coarse aerosols such as dust particles, which can affect the NIR wavelengths.

Difference between AOD products. Figure 7 shows the mean spatial differences of AOD derived from the satellite products (described in Section 2.2.1). There are distinct spatial differences in the mean spatial AOD difference maps as observed by MODIS, SEVIRI AERUS GEO, and MISR. From the spatial map of differences between SEVIRI AERUS GEO and MODIS (C-5.1 and C-6), we observe that MODIS AOD at 0.5 μm observed from both the collections (C-5.1 and C-6) are high when compared to AOD observed by SEVIRI AERUS GEO, especially over the southern Congo domain. Within the two MODIS AOD collection products C-6 and C-5.1, high AOD values are observed in C-6 (Figure 7e). The observed maximum differences in AOD between SEVIRI AERUS GEO and MODIS (Figure 7a,d,e) appear to match AOD observations of CAMS and MERRA especially over the regions of the Congo with a high aerosol load (Figure 4), showing disagreement under high aerosol conditions. The observations with MISR (Figure 7b,c,f) are not so obvious due to less frequent observations of AOD with MISR over this region. The percentages of successful AOD retrievals are calculated for various mentioned satellites and are tabulated in Table 2 for the year 2014. We only show here the statistics related to the latest MODIS collection C-6.

Due to the varying grid resolution between satellites MODIS (0.1°) and MISR (0.5°), it is most unlikely that the total number of computed pixels for the comparison is fixed and hence, as a result, the computed total number of pixels for MODIS. This MISR grid resolution is also different (see Table 2). It is clearly understood from Table 2 that the percentage of successful AOD retrievals for SEVIRI AERUS GEO is high with a value of more than 75% of the total pixels over the Congo domain. At the same time, the percentage of successful AOD retrievals for MODIS (C-6) and MISR are 17% and 3% of the total pixels respectively over the Congo domain. The percentage of successful AOD retrievals for MODIS (C-5.1) is observed to be higher with a value of 23%. Similar results were obtained from the comparison of SEVIRI derived AOD with MODIS and MISR over 24 AERONET stations around the Mediterranean sea in a study conducted by Xu et al. [43]. Table 2 indicates that the mean satellite-derived AOD values are observed to be 0.35 (MISR), 0.48 (MODIS) and 0.38 (SEVIRI AERUS GEO) over the domain and are quite comparable among each other. At the same time, the mean AOD at 550 nm value for CAMS (MERRA) is about 0.5 (0.3) (see Table 1, Figure 4). If a CAMS (MERRA) model derived AOD is used as a reference, the intercomparison between these two model-derived AOD's and 3 satellite-derived AODs indicates an overall uncertainty of around 0.1 for the mean AOD

value of 0.5 (20% in relative units). The same order of uncertainty (20%) exists between two successive collections of the same MODIS products (C-5.1 vs. C-6) as observed in Figure 8. The histogram of successful AOD retrievals observed from MODIS (C-6 and C-5.1) as a function of AOD bins is shown in Figure 8. The mean AOD value observed from MODIS (C-6) over the region of the Congo is high with a value of 0.48 compared with that of MODIS (C-5.1), which has a value of 0.40.

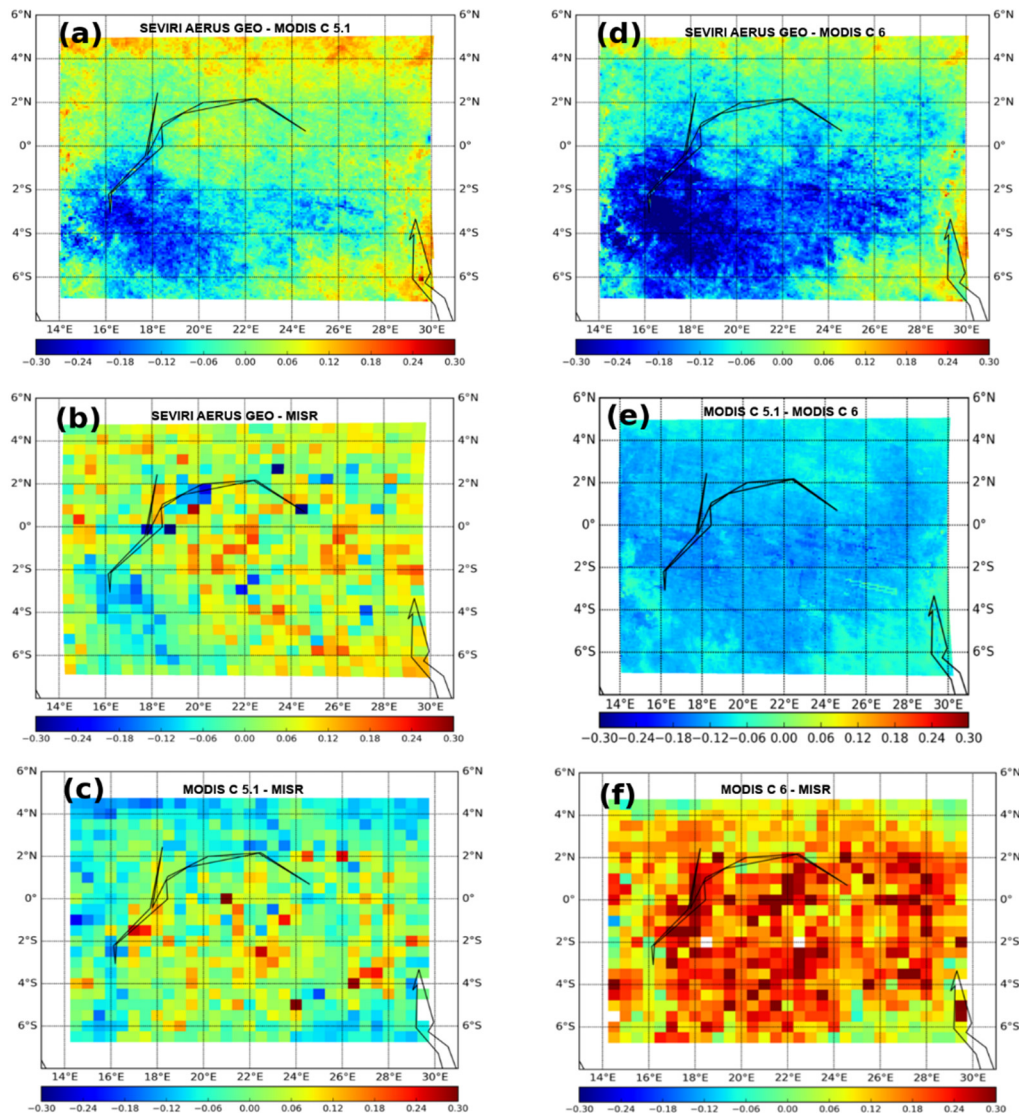


Figure 7. Spatial map of the average of the differences in AOD for various satellite pairs (a) SEVIRI AERUS GEO and MODIS (C-5.1), (b) SEVIRI AERUS GEO and MISR, (c) MODIS (C-5.1) and MISR, (d) SEVIRI AERUS GEO and MODIS (C-6), (e) MODIS C 5.1 and MODIS C-6 and (f) MODIS (C-6) and MISR. MODIS native grid resolution is 0.1 degrees and MISR native grid resolution is 0.5 degrees.

In deeper analysis, it is observed in Figure 8 that the histogram for MODIS (C-5.1) is centered over the AOD value 0.4 while it is shifted to a higher AOD value of nearly 0.5 for MODIS (C-6). From a study conducted by Georgoulias et al. [58], it was shown that C-6 MODIS products are significantly different to that of C-5.1 MODIS aerosol products when compared against AERONET observations over the Mediterranean region. From their study, there was a better agreement with C-6 (correlation of 0.87) compared to that of C-5.1 (correlation of 0.85) although the error associated with C-6 (RMSE of 0.081) was slightly higher than C-5.1 (RMSE of 0.076) [58]. The number of successful aerosol retrievals observed from C-6 MODIS is found to be higher (11%) than the AOD retrievals observed from C-5.1. Furthermore, Sayer et al. [59] in their study discussed that uncertainties in AOD products are found to

be similar with respect to the underlying surface type and aerosol models considered in C-6 MODIS and C-5.1 MODIS algorithms. In addition, their study also concluded that a high bias in AOD might present in the MODIS C-6 products for high-AOD conditions and for elevated regions [59].

Table 2. Contribution of successful AOD retrievals over the Congo region during the year 2014 for different satellites SEVIRI AERUS GEO, MODIS and MISR are detailed. The average AOD computed for the year 2014 from various satellites under varying grid resolution are also shown in the table.

SEVIRI AERUS GEO and MODIS C-6 (0.1-degree resolution)		
Number of pixels (N) = 9,379,040		
AOD product	Percentage of successful AOD retrievals (Observed samples)	Mean AOD
MODIS-DT	17% (1,683,725)	0.48
SEVIRI AERUS GEO	79% (7,441,795)	0.39
SEVIRI AERUS GEO and MISR (0.5-degree resolution)		
Number of pixels (N) = 294,190		
AOD product	Percentage of successful AOD retrievals (Observed samples)	Mean AOD
MISR	3% (10,002)	0.35
SEVIRI AERUS GEO	92% (272,360)	0.38
MODIS C-6 and MISR (0.5-degree resolution)		
Number of pixels (N) = 280,320		
AOD product	Percentage of successful AOD retrievals (Observed samples)	Mean AOD
MISR	3% (9561)	0.35
MODIS-DT	17% (50,102)	0.48

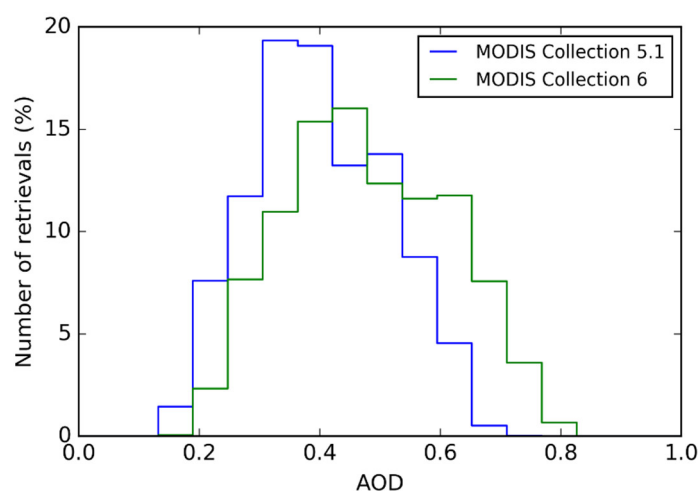


Figure 8. Histogram of successful AOD retrievals from MODIS (C-6 and C-5.1) products over the region of Congo, Africa. The legend is also shown for the respective products in the upper right corner of the figure.

3.3. Albedo Retrieval Sensitivity to AOD Uncertainty

3.3.1. Observational Perspective

It is observed from this study that spatial plots of surface albedo differences (Figure 6) share certain common patterns with respect to spatial plots of AOD differences (Figure 7). In order to investigate the relationship between the AOD bias and the surface albedo bias, a time series plot is constructed and

is shown in Figure 9. Each observational point in this daily time series plot corresponds to a spatial mean value of the corresponding observable variable over the region of the Congo. From Figure 9, it is observed that a high AOD bias (positive or negative) well corresponds to a highly visible albedo bias over the study region on a temporal scale. In addition, the AOD bias correlates strongly with visible albedo bias during the summer (June to September). However, a convincingly strong one to one correspondence between the two variables is not found (an overall correlation, R -value = -0.50 was only observed). The magnitude of the AOD bias shown in Figure 9 correlates positively with the average AOD of the atmosphere (see Figure 3), implying that satellite AOD products compare well for low AOD values of the atmosphere and diverge largely for high AOD values. The days corresponding to maximum AOD bias correlates with maximum visible albedo bias (June to September). The time series of NIR albedo bias is not shown as aerosols adversely impact the visible channel more than they do the NIR channel.

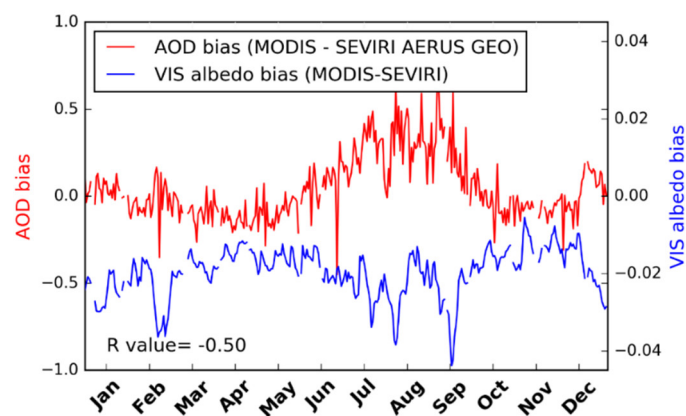


Figure 9. Time series of AOD bias and visible albedo bias over the region of Congo during the year 2014. Each point in both the temporal series corresponds to the spatial mean value of the observable variable over the study region.

3.3.2. Model Perspective

In this section, we investigate the relationship between AOD and surface albedo using a radiative transfer (RT) model. A sensitivity analysis is conducted by using an RT code to produce observation system simulation experiments (OSSE) based on the climatological environmental conditions over this study region. The model setup and simulations are explained hereafter.

Simulation with the 6S radiative transfer model. In order to observe the possible influence of varying aerosol conditions on the estimation of surface reflectance, the radiative transfer code 6S [60] is used in this study. The geometric conditions considered for the modeling include solar geometry, where solar zenith angle (SZA) is set to 45° , the solar azimuth angle (SAA) is set to 0° , the view geometry, where view zenith angle (VZA) is set to 0° and the view azimuth angle (VAA) is set to 0° .

All the simulations are carried out for a selected day (1st of July), at an elevation of 430 m, which is the average elevation of the Congo. A tropical atmospheric profile is considered. We consider a value of 0.5 for the AOD at 550 nm set according to the CAMS average over the region of study (see Figure 3b). Also, the aerosol layer considered in 6S is composed of 8% dust, 76% water soluble, 1% oceanic and 15% soot. Again, these values have been defined according to the average values observed by CAMS for the year 2014. The spectral wavelength specifications as given in the model for the VIS range are 0.4 to 0.7 μm . A homogeneous Lambertian surface with VIS albedo equal to 0.06 was used in the model, as this value is the mean spatial visible albedo observed value from SEVIRI over the region of the Congo during 2014.

3.3.3. Simulations—Two Sets of Simulations Are Run with the Radiative Transfer Code, 6S

Firstly, a forward simulation is carried out to calculate a realistic average of the radiance that is observed by SEVIRI over the Congo. Average surface reflectance and AOD at 550 nm are considered here for the simulation. This setup provided a TOA apparent radiance of $42.1 \text{ W/m}^2/\text{sr}/\mu\text{m}$ which will be used as a reference. Secondly, several inverse simulations (i.e., with atmospheric corrections) are performed starting from the previously calculated top-of-atmosphere radiance and considering all the other conditions are the same except for the aerosol content, which is based on purpose. Several runs are carried out with the following AOD values (0.125, 0.25, 0.375, 0.45, 0.5, 0.55, 0.625, 0.75, 0.875), which correspond to a bias in percentages of (−75, −50, −25, −10, 0, +10, +25, +50, +75). These inverse simulations allow us to study the relationship between the AOD bias and the precision of the retrieved surface reflectance.

Section 3.2 shows that there is around 20% uncertainty in the value of the AOD estimations (satellite and model-derived) over the Congo region with respect to the average AOD value of around 0.5. Figure 10 shows that this AOD uncertainty of 20% could lead to a surface reflectance uncertainty in the VIS of around 15% (see vertical and horizontal lines). The mean MSG surface reflectance (0.06; that is discussed in Section 3.1 earlier) is plotted with a dashed line.

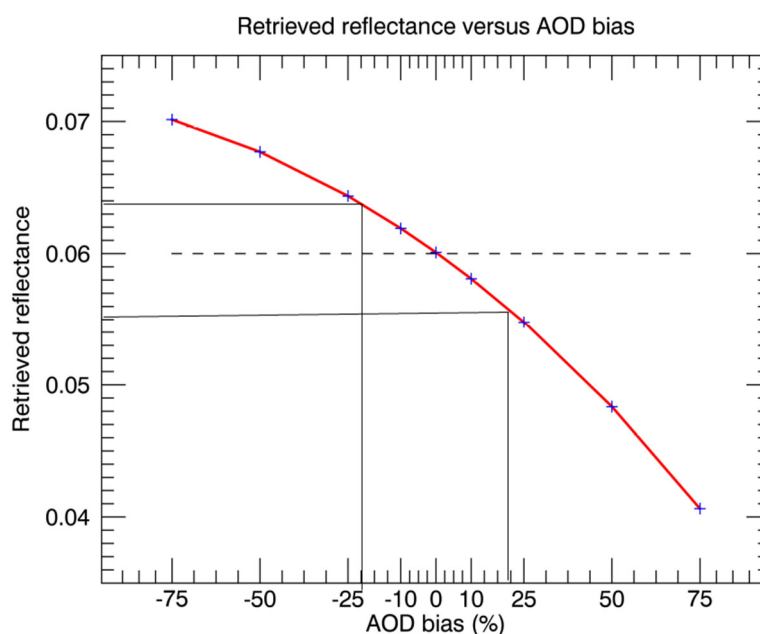


Figure 10. Retrieved surface reflectance error according to AOD bias observed from the 6S simulation. The dotted lines in the figure correspond to the average surface albedo value as observed from SEVIRI in VIS domain and that is used as input in the 6S simulations. The solid lines correspond to the bias estimated between CAMS and SEVIRI AERUS GEO AOD values.

In the same manner from this OSSE analysis, not accounting for the important AOD changes (up to +0.2 increase in AOD; see Figure 5) the result of volcano eruptions could lead to an artificial decrease of the surface albedo of around 25% in the VIS on a yearly basis over the Congo. As the effect of volcano emissions around the world usually leads to an AOD increase of more than 0.1 for a period of 2–3 years after the eruption, this artificial impact on surface albedo could prove to be important (16%) for the same period. And following the same logic, not accounting for the AOD increase for the last decade over this region (+14%) would lead to an artificial decrease of the surface albedo of around 8%. This study considers that the vegetation indices are calculated from the satellite albedo products without any temporal averaging. Hence, using any temporal averaging would reduce the final residual error in VI estimates.

4. Discussion

Forests play an important role in maintaining the ecological balance and hence remote sensing of forest vegetation is essential for achieving sustainable forest management [61,62]. Plants absorb the solar radiation between 400 and 700 nanometers through the chlorophyll pigments that are present on the leaf absorption surface [63]. This absorbed part of radiation, known as the absorbed photosynthetically active radiation (APAR) is known to relate with the differences in the visible and near-infrared regions of the solar energy spectrum and hence are often approximated by the vegetation indices [63,64]. The surface reflectance products that are used for the derivation of these vegetation indices, mainly NDVI, are highly dependent on the aerosol load of the atmosphere and therefore any residual aerosol contamination can introduce artifacts in the estimated variables [51,64–66]. In this regard, there is a need for the future scientific community to devise new methodologies that avoid the influence of aerosols and still be used for the study of vegetation characteristics. In this context, several recent studies show that emissivity contrast methods could circumvent this issue, and also offer accurate monitoring of the vegetation greenness [67]. These methods combine the satellite-derived vegetation indices along with the thermal emissivity index to classify the vegetation cover [67–70]. Having said that, the current study discusses these important aspects on the quality of satellite surface reflectance or surface albedo products. To address this, the discussion section is divided into three subsections and intermediate questions. First, we discuss whether or not the uncertainties in the albedo bias can be explained by using present-day satellite AOD products. Second, we discuss the changes in the surface albedo products with respect to the important AOD changes in the last three decades over the region of the Congo. Finally, we summarize and conclude the message of our study.

4.1. Can the Difference between Satellite Albedo Products Be Explained by AOD Uncertainty

From the current study, we observe that significant differences exist between various satellite products over the Congo. The overall minimum uncertainty observed between any two satellite AOD product pairs with respect to the mean AOD values observed from model aerosol products CAMS (MERRA) is around 20% (25%) respectively. The difference in sampling between the sensors that are on board geostationary and polar platforms may explain the most part of the difference in the satellite-derived estimates. This region is often cloudy in the afternoon and cloudiness is better tackled by the SEVIRI AOD product with MSG. AERUS-GEO AOD offers a successful retrieval for 80% of the days with AOD estimates available for less than 4% for MISR and 18% for MODIS-DT. With respect to the surface albedo observations, If MODIS is considered as a reference, the mean albedo values in the VIS (NIR) are observed as 0.04 (0.2) respectively. The relative difference between MODIS albedo and SEVIRI albedo across a major part of the study area, the Congo, is greater than +70% (−15%) in the VIS (NIR).

The question is whether an uncertainty of 20% in the AOD estimates could lead to an error of 70% in the retrieval of VIS albedo in this region. To address this question a sensitivity analysis was conducted through the use of a radiative transfer code to produce OSSE based on the climatological environmental condition across this region (Section 3.3). Figure 10 shows that the AOD uncertainty over this region ($0.5 \pm 20\%$) may explain up to 0.01 of changes in the retrieval of the surface reflectance in the VIS domain. Usually, the vegetation indices or surface albedo products that are estimated using the surface reflectance products consider compositing windows that can reduce the errors. However, studies report that regions with persistent cloud cover and high aerosol load such as the Congo rainforest can introduce errors in the surface reflectance data [64]. In conclusion, AOD uncertainty can only explain up to 15% (for the minimum AOD uncertainty between satellite products and model data sets) of the discrepancies between the surface albedo products in the VIS.

4.2. Would the Greenness (or Albedo Decrease) Be Possible If Important AOD Changes within in the Last Three Decades Are Not Taken into Account

It was observed from the MERRA modeling aerosol data that over the Congo there is a significant increase of dust aerosol type within the last three decades and an increase of black carbon and organic carbon over the past decade. This is the main reason behind an increase of 14% in the total AOD in the last decade between 2005 to 2015. Hence, we estimate that if this trend is not correctly taken into account in satellite retrieval methods for surface albedo, greenness of the surface properties (decrease of albedo) of around 8% could be artificially detected. Our study leaves the following important message over which to reflect regarding analysis studies of temporal trends in the satellite Climate Data Records: over very dense vegetation areas such as the Congo forest. The analysis of the greenness and brownness of the vegetation by using satellite variables [55] have to make sure that the existing AOD trends have been correctly taken into account in the atmospheric correction process.

4.3. Can We Detect the Vegetation Brownness or Greenness of Forests Using Satellite Surface Albedo Products

Over the Congo, if a negative trend of more than 10% is observed in the VIS surface albedo over the last 3 decades, we can affirm that the decrease (or vegetation greenness) is not due to aerosols uncertainties and hence not artificial. If a positive trend is observed in the VIS surface albedo over the last three decades, we can affirm that the increase (or brownness) is relevant whatever the value of the trend (as long as the latter is significant in a statistical sense). This is true however only if the following two assumptions are made: (1) the existence of reference measurements with a high accuracy of surface properties by satellite and (2) accurate AOD estimates (required for the satellite retrieval methods) exist. We proved that this is not the case over the Congo region, as AOD uncertainty (20%) can only explain up to 15% of the discrepancies between the surface albedos products in the VIS band. Accurate AOD estimates are essential for this kind of study but over the Congo in Africa, there are no ground stations for such accurate AOD measurements. The nearest one is at "SEGC_Lope_Gabon" and it doesn't lie in the center of the study region, in the Congo. Through this study, we propose to the scientific community the establishment of an AERONET station across this region.

5. Conclusions

The satellite-derived surface albedo (or reflectance) products are used extensively within the scientific community so as to address several scientific problems. It is however important for the users to understand the uncertainties associated with these satellite products. Some uncertainties arise due to the contamination of surface albedo caused by atmospheric residues coming from a limited atmospheric correction mainly due to a wrong characterization of aerosols. Furthermore, differences may exist between products coming from distinct satellites due to differences in acquisition geometry between polar-orbiting and geostationary satellites. In the context of the ever-increasing availability of satellite-derived products and climate data records nowadays, the current study emphasizes the importance of understanding aerosol uncertainties in order to address the differences in the satellite-derived surface albedo products. We have used both satellite observations and model outputs in order to understand this important problem. From our study, we show that with current satellite AOD products, a minimum uncertainty of around 20% exists between the current day satellite AOD product pairs. We estimate that this AOD uncertainty may explain only up to 15% changes in the observed 70% changes of the surface albedo products. We show that over the region of Congo, there is a significant increase of dust aerosol occurred in the past three decades. Also, there is an increase of total AOD of up to 14% in the last decade. From the modeling study, we estimate that this 14% increase in AOD could bring changes up to 0.005 in the surface albedo. The mean surface albedo value is about 0.06 over the region of Congo (see Section 3.1). Consequently, if this increase in the total AOD trend is not considered, we estimate a decrease of albedo or greenness of up to 8% (0.005/0.06) that can be artificially detected over the Congo region. We show that the satellite products of surface albedo can be used to detect the existing trends in vegetation if the accuracy of the satellite products is high. This can

be achieved if the AOD used in the atmospheric correction that provides surface albedo is also of high quality. We also showed that during a volcano eruption, the mean AOD could increase as much as by 40% (even if the volcano eruption took place thousands of miles from the studied area). Hence, neglecting these strong aerosol emissions could induce an artificial greenness (albedo decrease) of more than 25% in the year following the eruption. It is worth mentioning that satellite-derived surface reflectance products differ to the ground reality for all the several factors said above including the contamination due to residual aerosol effects. These factors may become important for the observed bias within the satellite-derived surface reflectance products. Hence, comparing the satellite reflectance products with the ground truth is only the viable method for understanding this exact bias. At the same time, the retrieval methods to derive these surface reflectance products also rely on a true estimate of aerosol load to understand and reduce the associated bias within the satellite-derived products. However, over this study region, there are no observations for estimating the ground reality of true surface reflectance and aerosol load. Hence without any such true observations, it would be a limitation for the scientific community for properly understanding the changes in surface greenness or brownness. Through this study, we propose to the scientific community for the establishment of ground stations over the study region, Congo, to properly quantify the changes in vegetation with respect to satellite products. To conclude, we believe that the analysis of shifts in vegetation properties by using the existing satellite-derived surface albedo or reflectance, and thus the vegetation indexes that exploit observations in VIS domain, are still quite questionable over tropical rainforest regions. This study can be extrapolated as well to other study regions, where the adverse impact of aerosols in the atmosphere could hinder the potential use of the surface albedo for scientific studies.

Author Contributions: D.C. conceptualized the initial idea for the experiment, D.C. and S.M. framed the methodology, S.M. performed the validation experiments, X.C. performed the modeling experiments, S.M., D.C., and X.C. analyzed the results, S.M. wrote the original draft of the article, S.M., D.C., and X.C. reviewed and edited the article.

Funding: This research was partially funded by EUMETSAT through a federated activity in the framework of the LSA-SAF project.

Acknowledgments: Authors thank the ICARE/AERIS team for the providing the AOD data from SEVIRI AERUS-GEO. We also thank C. Planque for her assistance and the LSA-SAF team for providing the surface albedo data.

Conflicts of Interest: The authors declare no conflict of interest.

References

1. Myers, N. (Ed.) *Tropical Forests and Climate*; Kluwer Academic: Dordrecht, The Netherland; Boston, MA, USA, 1992.
2. Loomis, I. Trees in the Amazon make their own rain. *Science* **2017**. [[CrossRef](#)]
3. Zhou, L.; Tian, Y.; Myneni, R.B.; Ciais, P.; Saatchi, S.; Liu, Y.Y.; Piao, S.; Chen, H.; Vermote, E.F.; Song, C.; et al. Widespread decline of Congo rainforest greenness in the past decade. *Nature* **2014**, *509*, 86–90. [[CrossRef](#)] [[PubMed](#)]
4. Johnson, B.T.; Shine, K.P.; Forster, P.M. The semi-direct aerosol effect: Impact of absorbing aerosols on marine stratocumulus. *Q. J. R. Meteorol. Soc.* **2004**, *130*, 1407–1422. [[CrossRef](#)]
5. Kaufman, Y.J.; Tanre, D.; Boucher, O. A satellite view of aerosols in the climate system. *Nature* **2002**, *419*, 215–223. [[CrossRef](#)] [[PubMed](#)]
6. Hodnebrog, Ø.; Myhre, G.; Forster, P.M.; Sillmann, J.; Samset, B.H. Local biomass burning is a dominant cause of the observed precipitation reduction in southern Africa. *Nat. Commun.* **2016**, 11236. [[CrossRef](#)] [[PubMed](#)]
7. Coe, M.T.; Marthews, T.R.; Costa, M.H.; Galbraith, D.R.; Greenglass, N.L.; Imbuzeiro, H.M.A.; Levine, N.M.; Malhi, Y.; Moorcroft, P.R.; et al. Deforestation and climate feedbacks threaten the ecological integrity of south-southeastern Amazonia. *Philos. Trans. R. Soc. B Biol. Sci.* **2013**, 368. [[CrossRef](#)] [[PubMed](#)]

8. Aragao, L.E.O.; Malhi, Y.; Barbier, N.; Lima, A.; Shimabukuro, Y.; Anderson, L.; Saatchi, S. Interactions between rainfall, deforestation and fires during recent years in the Brazilian Amazonia. *Philos. Trans. R. Soc. B Biol. Sci.* **2008**, *363*, 1779–1785. [[CrossRef](#)]
9. Atkinson, P.M.; Dash, J.; Jeganathan, C. Amazon vegetation greenness as measured by satellite sensors over the last decade: Decadal changes in Amazon Greenness. *Geophys. Res. Lett.* **2011**, *38*. [[CrossRef](#)]
10. Franklin, S.E. *Remote Sensing for Sustainable Forest Management*; CRC press: Boca Raton, FL, USA, 2000.
11. Huete, A.; Justice, C.; Leeuwen, W.V. *Modis Vegetation Index (MOD 13) Algorithm Theoretical Basis Document Version 3*; EOS Project Office; version-3; 1999. Available online: https://modis.gsfc.nasa.gov/data/atbd/atbd_mod13.pdf (accessed on 28 February 2019).
12. Franch, B.; Vermote, E.F.; Sobrino, J.A.; Fédèle, E. Analysis of directional effects on atmospheric correction. *Remote Sens. Environ.* **2013**, *128*, 276–288. [[CrossRef](#)]
13. Suman, M.N.S.; Gadhavi, H.; Kiran, V.R.; Jayaraman, A.; Rao, S.V.B. Role of Coarse and Fine Mode Aerosols in MODIS AOD Retrieval: A case study over southern India. *Atmos. Meas. Tech.* **2014**, *7*, 907–917. [[CrossRef](#)]
14. Mielonen, T.; Levy, R.C.; Aaltonen, V.; Komppula, M.; de Leeuw, G.; Huttunen, J.; Lihavainen, H.; Kolmonen, P.; Lehtinen, K.E.J.; Arola, A. Evaluating the assumptions of surface reflectance and aerosol type selection within the MODIS aerosol retrieval over land: The problem of dust type selection. *Atmos. Meas. Tech.* **2011**, *4*, 201–214. [[CrossRef](#)]
15. Kim, M.; Kim, J.; Wong, M.S.; Yoon, J.; Lee, J.; Wu, D.; Chan, P.W.; Nichol, J.E.; Chung, C.-Y.; Ou, M.-L. Improvement of aerosol optical depth retrieval over Hong Kong from a geostationary meteorological satellite using critical reflectance with background optical depth correction. *Remote Sens. Environ.* **2014**, *142*, 176–187. [[CrossRef](#)]
16. Cescatti, A.; Marcolla, B.; Vannan, S.K.S.; Pan, J.Y.; Román, M.O.; Yang, X.; Ciaia, P.; Cook, R.B.; Law, B.E.; Matteucci, G.; et al. Intercomparison of MODIS albedo retrievals and in situ measurements across the global FLUXNET network. *Remote Sens. Environ.* **2012**, *121*, 323–334. [[CrossRef](#)]
17. Seidel, F.C.; Popp, C. Critical surface albedo and its implications to aerosol remote sensing. *Atmos. Meas. Tech.* **2012**, *5*, 1653–1665. [[CrossRef](#)]
18. Jethva, H.; Satheesh, S.K.; Srinivasan, J.; Levy, C.R. Improved retrieval of aerosol size-resolved properties from moderate resolution imaging spectroradiometer over India: Role of aerosol model and surface reflectance. *J. Geophys. Res.* **2010**, *115*. [[CrossRef](#)]
19. Ceamanos, X.; Carrer, D.; Roujean, J.-L. Improved retrieval of direct and diffuse downwelling surface shortwave flux in cloudless atmosphere using dynamic estimates of aerosol content and type: Application to the LSA-SAF project. *Atmos. Chem. Phys.* **2014**, *14*, 8209–8232. [[CrossRef](#)]
20. Fensholt, R.; Sandholt, I.; Stisen, S.; Tucker, C. Analysing NDVI for the African continent using the geostationary meteosat second generation SEVIRI sensor. *Remote Sens. Environ.* **2006**, *101*, 212–229. [[CrossRef](#)]
21. Hilker, T.; Lyapustin, A.I.; Tucker, C.J.; Sellers, P.J.; Hall, F.G.; Wang, Y. Remote sensing of tropical ecosystems: Atmospheric correction and cloud masking matter. *Remote Sens. Environ.* **2012**, *127*, 370–384. [[CrossRef](#)]
22. Anderson, L.O.; Malhi, Y.; Aragão, L.E.O.C.; Ladle, R.; Arai, E.; Barbier, N.; Phillips, O. Remote sensing detection of droughts in Amazonian forest canopies. *New Phytol.* **2010**, *187*, 733–750. [[CrossRef](#)] [[PubMed](#)]
23. Amri, R.; Zribi, M.; Lili-Chabaane, Z.; Duchemin, B.; Gruhier, C.; Chehbouni, A. Analysis of Vegetation Behavior in a North African Semi-Arid Region, Using SPOT-VEGETATION NDVI Data. *Remote Sens.* **2011**, *3*, 2568–2590. [[CrossRef](#)]
24. Xu, L.; Samanta, A.; Costa, M.H.; Ganguly, S.; Nemani, R.R.; Myneni, R.B. Widespread decline in greenness of Amazonian vegetation due to the 2010 drought. *Geophys. Res. Lett.* **2011**, *38*, L07402. [[CrossRef](#)]
25. Jeong, S.-J.; Ho, C.-H.; Jeong, J.-H. Increase in vegetation greenness and decrease in springtime warming over east Asia: Vegetation Weaken Regional Warming. *Geophys. Res. Lett.* **2009**, *36*. [[CrossRef](#)]
26. Mutanga, O.; Skidmore, A.K. Narrow band vegetation indices overcome the saturation problem in biomass estimation. *Int. J. Remote Sens.* **2004**, *25*, 3999–4014. [[CrossRef](#)]
27. Huete, A.R.; Liu, H.Q.; Batchily, K.; van Leeuwen, W. A comparison of vegetation indices over a global set of TM images for EOS-MODIS. *Remote Sens. Environ.* **1997**, *59*, 440–451. [[CrossRef](#)]
28. Vargas, M.; Kogan, F.; Guo, W. Empirical normalization for the effect of volcanic stratospheric aerosols on AVHRR NDVI. *Geophys. Res. Lett.* **2009**, *36*, L07701. [[CrossRef](#)]
29. Planque, C.; Carrer, D.; Roujean, J.-L. Analysis of MODIS albedo changes over steady woody covers in France during the period of 2001–2013. *Remote Sens. Environ.* **2017**, *191*, 13–29. [[CrossRef](#)]

30. Geiger, B.; Carrer, D.; Franchisteguy, L.; Roujean, J.-L.; Meurey, C. Land Surface Albedo Derived on a Daily Basis From Meteosat Second Generation Observations. *IEEE Trans. Geosci. Remote Sens.* **2008**, *46*, 3841–3856. [[CrossRef](#)]
31. Carrer, D.; Roujean, J.-L.; Meurey, C. Comparing Operational MSG/SEVIRI Land Surface Albedo Products From Land SAF With Ground Measurements and MODIS. *IEEE Trans. Geosci. Remote Sens.* **2010**, *48*, 1714–1728. [[CrossRef](#)]
32. Wanner, W.; Strahler, A.H.; Hu, B.; Lewis, P.; Muller, J.-P.; Li, X.; Schaaf, C.L.B.; Barnsley, M.J. Global retrieval of bidirectional reflectance and albedo over land from EOS MODIS and MISR data: Theory and algorithm. *J. Geophys. Res. Atmos.* **1997**, *102*, 17143–17161. [[CrossRef](#)]
33. Lucht, W.; Schaaf, C.B.; Strahler, A.H. An algorithm for the retrieval of albedo from space using semiempirical BRDF models. *IEEE Trans. Geosci. Remote Sens.* **2000**, *38*, 977–998. [[CrossRef](#)]
34. Schaaf, C.B.; Gao, F.; Strahler, A.H.; Lucht, W.; Li, X.; Tsang, T.; Strugnell, N.C.; Zhang, X.; Jin, Y.; Muller, J.-P.; et al. First operational BRDF, albedo nadir reflectance products from MODIS. *Remote Sens. Environ.* **2002**, *83*, 135–148. [[CrossRef](#)]
35. Vermote, E.F.; el Saleous, N.; Justice, C.O.; Kaufman, Y.J.; Privette, J.L.; Remer, L.; Roger, J.C.; Tanré, D. Atmospheric correction of visible to middle-infrared EOS-MODIS data over land surfaces: Background, operational algorithm and validation. *J. Geophys. Res. Atmos.* **1997**, *102*, 17131–17141. [[CrossRef](#)]
36. Vermote, E.F.; Vermeulen, A. Algorithm Theoretical Basis Document (ATBD) for the Atmospheric Correction Algorithm: Spectral Reflectances (MOD09). *ATBD Version* **1999**, *4*, 1–7.
37. Levy, R.C.; Mattoo, S.; Munchak, L.A.; Remer, L.A.; Sayer, A.M.; Patadia, F.; Hsu, N.C. The Collection 6 MODIS aerosol products over land and ocean. *Atmos. Meas. Tech.* **2013**, *6*, 2989–3034. [[CrossRef](#)]
38. Levy, R.C.; Remer, L.A.; Kleidman, R.G.; Mattoo, S.; Ichoku, C.; Kahn, R.; Eck, T.F. Global evaluation of the Collection 5 MODIS dark-target aerosol products over land. *Atmos. Chem. Phys.* **2010**, *10*, 10399–10420. [[CrossRef](#)]
39. Diner, D.J.; Martonchik, J.V.; Kahn, R.A.; Pinty, B.; Gobron, N.; Nelson, D.L.; Holben, B.N. Using angular and spectral shape similarity constraints to improve MISR aerosol and surface retrievals over land. *Remote Sens. Environ.* **2005**, *94*, 155–171. [[CrossRef](#)]
40. Kahn, R.A.; Gaitley, B.J.; Martonchik, J.V.; Diner, D.J.; Crean, K.A.; Holben, B. Multiangle Imaging Spectroradiometer (MISR) global aerosol optical depth validation based on 2 years of coincident Aerosol Robotic Network (AERONET) observations. *J. Geophys. Res. Atmos.* **2005**, *110*, D10S04. [[CrossRef](#)]
41. Carrer, D.; Roujean, J.-L.; Hautecoeur, O.; Elias, T. Daily estimates of aerosol optical thickness over land surface based on a directional and temporal analysis of SEVIRI MSG visible observations. *J. Geophys. Res. Atmos.* **2010**, *115*, D10208. [[CrossRef](#)]
42. Carrer, D.; Ceamanos, X.; Six, B.; Roujean, J.-L. AERUS-GEO: A newly available satellite-derived aerosol optical depth product over Europe and Africa. *Geophys. Res. Lett.* **2014**, *41*, 7731–7738. [[CrossRef](#)]
43. Xu, H.; Ceamanos, X.; Roujean, J.-L.; Carrer, D.; Xue, Y. Can satellite-derived aerosol optical depth quantify the surface aerosol radiative forcing? *Atmos. Res.* **2014**, *150*, 151–167. [[CrossRef](#)]
44. Nabat, P.; Somot, S.; Mallet, M.; Michou, M.; Sevault, F.; Driouech, F.; Meloni, D.; di Sarra, A.; Di Biagio, C.; Formenti, P. Dust aerosol radiative effects during summer 2012 simulated with a coupled regional aerosol-atmosphere-ocean model over the mediterranean region. *Atmos. Chem. Phys. Discuss.* **2014**, *14*, 25351–25410. [[CrossRef](#)]
45. Eskes, H.; Huijnen, V.; Arola, A.; Benedictow, A.; Blechschmidt, A.-M.; Botek, E.; Boucher, O.; Bouarar, I.; Chabrillat, S.; Cuevas, E.; et al. Validation of reactive gases and aerosols in the MACC global analysis and forecast system. *Geosci. Model Dev.* **2015**, *8*, 3523–3543. [[CrossRef](#)]
46. Cuevas, E.; Camino, C.; Benedetti, A.; Basart, S.; Terradellas, E.; Baldasano, J.M.; Morcrette, J.J.; Marticorena, B.; Goloub, P.; Mortier, A.; et al. The MACC-II 2007–2008 reanalysis: Atmospheric dust evaluation and characterization over northern Africa and the Middle East. *Atmos. Chem. Phys.* **2015**, *15*, 3991–4024. [[CrossRef](#)]
47. Eskes, H.J.; Wagner, A.; Schulz, M.; Christophe, Y.; Ramonet, M.; Basart, S.; Benedictow, A.; Lechschmidt, A.-M.B.; Chabrillat, S.; Clark, H. Validation Report of the CAMS near real time Global Atmospheric Composition Service. In *System Evolution and Performance Statistics; Status upto 1 September 2016 Copernicus Atmosphere Monitoring Service (CAMS) Report*; 2016. Available online: https://atmosphere.copernicus.eu/sites/default/files/repository/CAMS84_2015SC1_D84.1.5_201611_v1_0.pdf (accessed on 28 February 2019).

48. Jacker, J.G.; Leptoukh, G. Online Analysis Enhances Use of NASA Earth Science Data. *Trans. Am. Geophys. Union* **2007**, *88*, 14–17.
49. Veselovskii, I.; Goloub, P.; Podvin, T.; Tanre, D.; da Silva, A.; Colarco, P.; Castellanos, P.; Korenskiy, M.; Hu, Q.; Whiteman, D.N.; et al. Characterization of smoke and dust episode over West Africa: Comparison of MERRA-2 modeling with multiwavelength Mie–Raman lidar observations. *Atmos. Meas. Tech.* **2018**, *11*, 949–969. [[CrossRef](#)]
50. Rienecker, M.M.; Suarez, M.J.; Gelaro, R.; Todling, R.; Bacmeister, J.; Liu, E.; Bosilovich, M.G.; Schubert, S.D.; Takacs, L.; Kim, G.-K.; et al. MERRA: NASA’s Modern-Era Retrospective Analysis for Research and Applications. *J. Clim.* **2011**, *24*, 3624–3648. [[CrossRef](#)]
51. Buchard, V.; da Silva, A.M.; Randles, C.A.; Colarco, P.; Ferrare, R.; Hair, J.; Hostetler, C.; Tackett, J.; Winker, D. Evaluation of the surface PM_{2.5} in Version 1 of the NASA MERRA Aerosol Reanalysis over the United States. *Atmos. Environ.* **2016**, *125*, 100–111. [[CrossRef](#)]
52. Buchard, V.; da Silva, A.M.; Colarco, P.R.; Darmenov, A.; Randles, C.A.; Govindaraju, R.; Torres, O.; Campbell, J.; Spurr, R. Using the OMI aerosol index and absorption aerosol optical depth to evaluate the NASA MERRA Aerosol Reanalysis. *Atmos. Chem. Phys.* **2015**, *15*, 5743–5760. [[CrossRef](#)]
53. Lee, K.H.; Li, Z.; Kim, Y.J.; Kokhanovsky, A. Atmospheric Aerosol Monitoring from Satellite Observations: A History of Three Decades. *Atmos. Biol. Environ. Monit.* **2009**, *13*. [[CrossRef](#)]
54. Mao, K.B.; Ma, Y.; Xia, L.; Chen, W.Y.; Shen, X.Y.; He, T.J.; Xu, T.R. Global aerosol change in the last decade: An analysis based on MODIS data. *Atmos. Environ.* **2014**, *94*, 680–686. [[CrossRef](#)]
55. Lee, H.; Kalashnikova, O.V.; Suzuki, K.; Braverman, A.; Garay, M.J.; Kahn, R.A. Climatology of the aerosol optical depth by components from the Multi-angle Imaging SpectroRadiometer (MISR) and chemistry transport models. *Atmos. Chem. Phys.* **2016**, *16*, 6627–6640. [[CrossRef](#)]
56. Tummon, F.; Solmon, F.; Liousse, C.; Tadzross, M. Simulation of the direct and semidirect aerosol effects on the southern Africa regional climate during the biomass burning season. *J. Geophys. Res.* **2010**, *115*. [[CrossRef](#)]
57. Chin, M.; Diehl, T.; Tan, Q.; Prospero, J.M.; Kahn, R.A.; Remer, L.A.; Yu, H.; Sayer, A.M.; Bian, H.; Geogdzhayev, I.V.; et al. Multi-decadal aerosol variations from 1980 to 2009: A perspective from observations and a global model, *Atmos. Chem. Phys.* **2014**, *14*, 3657–3690. [[CrossRef](#)]
58. Georgoulias, A.K.; Alexandri, G.; Kourtidis, K.A.; Lelieveld, J.; Zanis, P.; Amiridis, V. Differences between the MODIS Collection 6 and 5.1 aerosol datasets over the greater Mediterranean region. *Atmos. Environ.* **2016**, *147*, 310–319. [[CrossRef](#)]
59. Sayer, A.M.; Hsu, N.C.; Bettenhausen, C.; Jeong, M.-J. Validation and uncertainty estimates for MODIS Collection 6 ‘Deep Blue’ aerosol data: Deep Blue Collection 6 Validation. *J. Geophys. Res. Atmos.* **2013**, *118*, 7864–7872. [[CrossRef](#)]
60. Vermote, E.F.; Tanre, D.; Deuze, J.L.; Herman, M.; Morcette, J.-J. Second Simulation of the Satellite Signal in the Solar Spectrum, 6S: An overview. *IEEE Trans. Geosci. Remote Sens.* **1997**, *35*, 675–686. [[CrossRef](#)]
61. Chiteculo, V.; Abdollahnejad, A.; Panagiotidis, D.; Surovy, P.; Sharma, R.P. Defining Deforestation Patterns Using Satellite Images from 2000 and 2017: Assessment of Forest Management in Miombo Forests—A Case Study of Huambo Province in Angola. *Sustainability* **2019**, *11*, 98. [[CrossRef](#)]
62. Coops, N.C.; Hilker, T.; Hall, F.G.; Nichol, C.J.; Drolet, G.G. Estimation of Light-use Efficiency of Terrestrial Ecosystems from Space: A Status Report. *BioScience* **2010**, *60*, 788–797. [[CrossRef](#)]
63. Samanta, A.; Ganguly, S.; Vermote, E.; Nemani, R.R.; Myneni, R.B. Why Is Remote Sensing of Amazon Forest Greenness So Challenging? *Earth Interact.* **2012**, *16*, 1–14. [[CrossRef](#)]
64. Lim, H.; Choi, M.; Kim, J.; Kasai, Y.; Chan, P.W. AHI/Himawari-8 Yonsei Aerosol Retrieval (YAER): Algorithm, Validation and Merged Products. *Remote Sens.* **2018**, *10*, 699. [[CrossRef](#)]
65. Xiao, X.; Braswell, B.; Zhang, Q.; Boles, S.; Frolking, S.; Moore, B. Sensitivity of vegetation indices to atmospheric aerosols: Continental-scale observations in Northern Asia. *Remote Sens. Environ.* **2003**, *84*, 385–392. [[CrossRef](#)]
66. French, A.N.; Schmugge, T.J.; Kustas, W.P. Discrimination of Senescent Vegetation Using Thermal Emissivity Contrast. *Remote Sens. Environ.* **2000**, *74*, 249–254. [[CrossRef](#)]
67. Borbas, E.E.; Hulley, G.; Feltz, M.; Knuteson, R.; Hook, S. The Combined ASTER MODIS Emissivity over Land (CAMEL) Part 1: Methodology and High Spectral Resolution Application. *Remote Sens.* **2018**, *10*, 643. [[CrossRef](#)]

68. Masiello, G.; Serio, C.; De Feis, I.; Amoroso, M.; Venafra, S.; Trigo, I.F.; Watts, P. Kalman filter physical retrieval of surface emissivity and temperature from geostationary infrared radiances. *Atmos. Meas. Tech.* **2013**, *6*, 3613–3634. [[CrossRef](#)]
69. Masiello, G.; Serio, C.; Venafra, S.; Liuzzi, G.; Göttsche, F.; Trigo, I.F.; Watts, P. Kalman filter physical retrieval of surface emissivity and temperature from SEVIRI infrared channels: A validation and intercomparison study. *Atmos. Meas. Tech.* **2015**, *8*, 2981–2997. [[CrossRef](#)]
70. Alba, E.; Pereira, R.S.; Marchesan, J.; Silva, E.A.; de Batista, F.; Kazama, V.S.; Schuh, M.S.; Spiazzi, J.A. Albedo Trend Analyses in Atlantic Forest Biome Areas. *J. Agric. Sci.* **2018**, *10*, 298–307. [[CrossRef](#)]



© 2019 by the authors. Licensee MDPI, Basel, Switzerland. This article is an open access article distributed under the terms and conditions of the Creative Commons Attribution (CC BY) license (<http://creativecommons.org/licenses/by/4.0/>).